International Journal of Concrete Structures and Materials
Vol.2, No.2, pp. 115~122, December 2008

On the Ductility of High-Strength Concrete Beams

Il-Young Jang,[1)] Hoon-Gyu Park,[2)] Sung-Soo Kim,[3)] Jong-Hoe Kim,[4)] and Yong-Gon Kim[5)]

(Received May 18, 2008, Revised September 30, 2008, Accepted October 30, 2008)

Abstract : Ductility is important in the design of reinforced concrete structures. In seismic design of reinforced concrete members, it is necessary to allow for relatively large ductility so that the seismic energy is absorbed to avoid shear failure or significant degradation of strength even after yielding of reinforcing steels in the concrete member occurs. Therefore, prediction of the ductility should be as accurate as possible. The principal aim of this paper is to present the basic data for the ductility evaluation of reinforced high-strength concrete beams. Accordingly, 23 flexural tests were conducted on full-scale structural concrete beam specimens having concrete compressive strength of 40, 60, and 70 MPa. The test results were then reviewed in terms of flexural capacity and ductility. The effect of concrete compressive strength, web reinforcement ratio, tension steel ratio, and shear span to beam depth ratio on ductility were investigated experimentally.

Keywords : high-strength concrete, ductility, flexural behavior

1. Introduction

The current practice of structural member design recommends low tension steel ratio in order to ensure adequate ductility of the construction structure so that the necessary warning can be given prior to the failure of the member. Especially, the ductile failure mode is essential for the appropriate redistribution of the moment of earthquake-proof and statistically indeterminate structures. Thus, an experimental investigation to establish the relationship between the ductility and the flexural behavior of high-strength steel-concrete beam members with brittle failure tendency is required to ensure the necessary ductility.

Although this requirement can be met easily by lowering the tension steel ratio in order to ensure the ductility of the high-strength concrete members, there is a difficulty in obtaining the ultimate flexural strength.[1] Moreover, it can result in an uneconomical design by relatively enlarging the cross section of the structural member.

Thus, this study aims to delineate the relationship between the flexural behavior and the ductility of the member by carrying out a flexural load test on a test specimen with experimental variables of concrete compressive strength, tension steel ratio, etc. in order to investigate the flexural behavior of the high-strength concrete.

[1)]KCI Member, Dept. of Civil Engineering, Kumoh National University of Technology, Kumi 730-701, Korea. *E-mail: jbond@kumoh.ac.kr*
[2)]KCI Member, LIG E & C Corporation, Seoul 135-080, Korea.
[3)]Samsung C & T Corporation, Seoul 137-857, Korea.
[4)]Ministry of Land Transport and Maritime Affairs, Gwacheon 427-712, Korea.
[5)]KCI Member,Dept. of Safety Engineering, Hankyong National University, Ansung 456-949, Korea.

2. Experiment

2.1 Experimental plan

The overall details and specifications of the beam specimens and the reinforcing steel bars, which were prepared to investigate the ductility of high-strength concrete, are shown in Table 1 and Fig. 1. Since the force equilibrium equation can always be set up for the cross section of the beam member, the variables were selected based on the concept of equilibrium ratio so that the same ratio can be applied to both the tension steel ratio and equilibrium steel bar ratio including concrete compressive strength and the yield strength of the rebar. Thus, the equilibrium steel bar ratio of existing design standard, 0.75 ρ_b, and Leslie's 0.35 ρ_b, were set the standard with other equilibrium steel bar ratios of 1.0 ρ_b, 0.7 ρ_b, 0.5 ρ_b, and 0.3 ρ_b to be considered in this study. Here, the equilibrium steel bar ratio, ρ_b, was computed by the specification set forth by ACI-318 code, which is the current design equation. Two-point loading was applied to derive a pure flexural stress zone. Additionally, the shear span to beam depth ratios varied by 2.5, 3.2, and 4.0, and the shear span was reinforced by closed stirrups to avoid shear fracture. The concrete compressive strengths of the test specimens varied by 40, 60 and 70 MPa.

2.2 Test specimen preparation and materials test

2.2.1. Materials and test specimen preparation

Table 2 shows the concrete mixing proportion for the test specimens with experimentally planned compressive strengths of 40, 60, and 70 MPa to be used in the ductility evaluation of the high-strength concrete structural member.

ASTM type 1 ordinary Portland cement manufactured by domestic S company was used. The fine and coarse aggregate were obtained from the sand at the Nakdong river of average fineness modulus of 2.94 and macadam (coarse aggregate) of average fine-

Table 1 Test plan for high-strength concrete beams.

No.	Beam ID.	f_c MPa	Section (b×d) *mm*	a/d	Tension steel No.	Tension steel ρ_t(%)	$\frac{\rho_t}{\rho_b}$	Compression steel No.	Compression steel ρ_c(%)	$\frac{\rho_c}{\rho_t}$	$\frac{\rho_t \rho}{\rho_b}$	Web reinforcement No.	Web reinforcement s (mm)	Web reinforcement ρ_w(%)	Web reinforcement Shape
1	4B2-0.5	40	140 × 210		2D19	1.952	0.562	-	-	0	0				
2	6B2-0.5	60	140 × 210	2.5	2D19	1.952	0.435	-	-	0	0		100	1.021	
3	7B2-0.5	75	140 × 210		2D22	2.633	0.502	-	-	0	0				
4	4B3-0.05	40	250 × 300		2D10	0.200	0.055	-	-	0	0		70	0.817	
5	4B3-0.1	40	250 × 300		2D13	0.340	0.098	-	-	0	0				
6	4B3-0.5	40	140 × 210		2D19	1.952	0.562	-	-	0	0		100	1.021	
7	6B3-0.5	60	140 × 210	3.2	2D19	1.952	0.435	-	-	0	0				
8	7B3-0.05	75	250 × 300		2D13	0.340	0.065	-	-	0	0		70	0.817	
9	7B3-0.1	75	250 × 300		3D13	0.510	0.097	-	-	0	0				
10	7B3-0.5	75	140 × 210		2D22	2.633	0.502	-	-	0	0				
11	4B4-0.3	40	140 × 210		2D16	1.354	0.390	-	-	0	0				
12	4B4-0.5	40	140 × 210		2D19	1.952	0.562	-	-	0	0	D10			□
13	4B4-0.7	40	140 × 210		2D22	2.633	0.758	-	-	0	0				
14	4B4-0.7(C0.2)	40	140 × 210		2D22	2.633	0.758	2D10	0.486	0.185	0.618				
15	4B4-0.7(C0.3)	40	140 × 210		2D22	2.633	0.758	2D13	0.864	0.328	0.509				
16	4B4-1.0	40	140 × 195		4D19	4.205	1.211	-	-	0	0		100	1.021	
17	6B4-0.5	60	140 × 210	4.0	2D19	1.952	0.435	-	-	0	0				
18	7B4-0.3	71	140 × 210		2D19	1.952	0.373	-	-	0	0				
19	7B4-0.5	71	140 × 210		2D22	2.633	0.502	-	-	0	0				
20	7B4-0.7	71	140 × 195		4D19	4.205	0.803	-	-	0	0				
21	7B4-0.7(C0.2)	75	140 × 195		4D19	4.205	0.803	3D10	0.784	0.187	0.659				
22	7B4-0.7(C0.3)	75	140 × 195		4D19	4.205	0.803	1D22	1.418	0.337	0.532				
23	7B4-1.0	75	140 × 195		4D22	5.670	1.082	-	-	0	0				

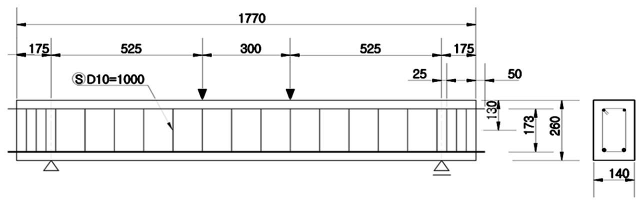

Fig. 1 Detail of test specimens (ex. 4B2-0.5, 6B2-0.5).

Table 2 Mixing proportion of high-strength concrete specimen.

Target compressive strength at 28 days (MPa)	40	60	70
W/B	0.480	0.358	0.250
S/A	0.437	0.413	0.390
Water (kg/m^3)	180	175	160
Cement (kg/m^3)	375	489	608
Gravel (kg/m^3)	997	991	1008
Sand (kg/m^3)	765	689	622
Silica fume (kg/m^3)	0	0	32
Super-plasticizer (kg/m^3)	0.43	0.65	2.33

ness modulus of 7.06, respectively. The silica hume replaced the cement by 10% in order to produce high-strength concrete. D10 rebars were mainly used as transverse reinforcing steel bars (stirrup), and SD40 (D10, D13, D19, and D22) were used as the main rebars. These rebars were placed in the test specimens by various tension steel ratios as specified in the experimental plan.

2.2.2. Tensile strength of rebar

As aforementioned, the rebars used in the test specimen were SBD40 (D10, D13, D19, and D22), and they were subjected to tensile strength test in accordance with the standard metal tensile strength test method. Table 3 and Table 4 show the mechanical properties of the rebar and the result of the strength tests on the test specimens, respectively.

2.2.3. Strength property of concrete

As the high-strength specimens were being prepared, compressive and splitting tensile test specimens of Φ100 × 200 mm size dimension, flexural test specimen of 150 × 150 × 550 mmsize, and bond strength test specimen of 150 × 150 × 150 mmsize were prepared as well. They were cured together with the test specimen under the same condition and were subjected to various strength tests at 28 days pursuant to KSF 2305, KSF 2423, KSF 2408, and ASTM, respectively.

Both ends of the test specimen were capped with sulfur to distribute the load more evenly and to minimize the eccentricity during the compressive strength test. The measured compressive strength was multiplied by 0.97, the value of calibration coeffi-

Table 3 Mechanical properties of steel.

Steel size	Yield strength f_{sy} (MPa)	Ultimate strength f_{su} (MPa)	Yield strain ε_{sy}	Modulus of Elasticity E_s (MPa)	Elongation (%)
D10	395	592	0.002054	192,350	23.4
D13	413	476	0.002036	203,040	16.3
D16	418	610	0.002153	194,270	24.0
D19	435	618	0.002064	210,760	21.2
D22	450	619	0.002042	220,450	19.5

Table 4 Strength properties of the concrete specimens

Properties			Target compressive strength (MPa)		
			40	60	70
Fresh	Slump	mm	160	130	150
Hardened	Age	day	28	28	53
	Compressive strength, f_c	MPa	41	61	71
	Splitting tensile strength, f_t	MPa	3.7	4.5	5.5
	Flexural strength, f_{cr}	MPa	4.9	6.1	6.4
	Max. bond strength-slip	MPa-mm	7.5-0.030	8.3-0.024	9.1-0.036
	Modulus of elasticity, E_c	MPa	27463	31750	32710

cient, to convert it appropriate for the standard test specimen of Φ150 × 300 mm dimension. The elasticity of modulus was measured pursuant to KSF 2438 and ASTM C 469-65.

The bond strength was measured by a UTM (Universal Test Machine) and load cell of 100tonf capacity on the test specimen with D22 steel bar of 15cm depth embedded in it to control the loading and to measure the load. The slip was measured by a dial gauge of 1/1,000 mm accuracy during the bond strength test. The strength test results are summarized in Table 4 below.

2.3 Experimental method

The loading test was conducted using a loading frame for structural experiment, and the load was measured by a load cell of 1,000 kN.

The load was applied through a loading device of H150 × 150 × 7 × 10 mm dimension while maintaining the platen-to-platen distance of 300 mm as illustrated in Fig. 2. As the load is applied, three LVDT's, which were installed at the center and 200 mm away on the left and right side of the center, measured the deflection of the beam specimen. Additionally, the compressive strain of the concrete at the flexural region, the strain on the tension steel, and the stirrup strain at the location of the distance *d* (the effective height of the beam) away from the shear-risk region were measured. The strains of the main tension steel and stirrup were measured by strain gauges. Three LVDT's were installed centering on the beam center and 2*d* (twice the effective height of the beam) distance away from the center to measure the strains at the upper and lower part of the concrete in flexural region and the curvature and rotation in the plastic hinge region. While the experiment was in progress, the crack patterns by each loading stage were directly traced on the beam.

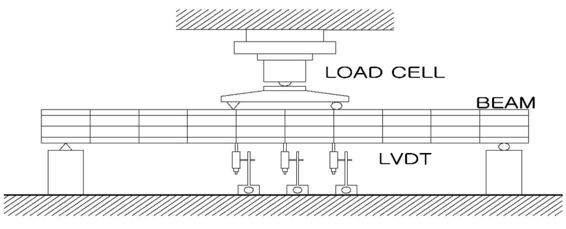

Fig. 2 Loading equipment.

2.4 Experimental result

2.4.1. Load-deflection relationship

The principal objective of this experiment is to observe and quantify the change in the flexural strength and ductility in response to the experimental variables of tension steel ratio, shear span ratio, etc. for the beam member of high-strength concrete. Accordingly, reinforcing rebars against flexure and shear were installed in all test specimens in accordance with the actual design standards.

The experimental result revealed that all test specimens reached or exceeded the expected flexural strength, and the experimental results for each test specimen are summarized by the loading step in Table 5.

In table 5, P_{cr} indicates the applied load during initial flexural crack, and the yield state represents the behavior of the member at the yield state (yield load P_y, deflection during the yield state δ_y, and maximum compressive strain on the concrete ε_{cy}). Here, the yield state of the member was defined by 75% secant method, which used the secant line connecting the origin of the load-deflection curve and 75% maximum load, to express the load and displacement at the yield state point. P_{sy} represents the load value at the tension steel yield point.

The maximum state represents the load ($P_{\max}$), deflection ($\delta_{\max}$), and maximum compressive strain on the concrete ε_{cmax}) at the maximum loading point. Ultimate state means the behavior of the beam member specimen after the maximum loading, and the ultimate load and displacement at 90% and 80% of the maximum loading are symbolized as P_{u1}, δ_{u1} and P_{u2}, δ_{u2}, respectively. ε_{cu} represents maximum compressive strain on the concrete after ε_{cmax} and until the failure of the member. It can be expressed as the ultimate strain on the concrete beam member at the compressive side subjected to flexural force of 0.003, which is the maximum compressive strain on the concrete often used in the design and analysis of flexural member. The result of load-deflection experiment is discussed at length in section 3.

2.4.2. Crack propagation pattern of the specimen under maximum load

Typical crack occurrence/propagation and failure pattern are shown in Fig. 3. As the shear span is shorter and the tension steel ratio is lower, the neutral axis at the pure bending zone ascended almost to the lower end of the compression zone, as shown by the crack propagation just prior to the failure of the test specimen. Additionally, when the specimen member possesses greater concrete compressive strength or greater amount of tension steel, its crack showed a pattern of narrower and complex crack as well as wider failure area on the compressive side. At the flexural shear region, the main crack propagated vertically regardless of the tension steel ratio. As the tension steel ratio increased, diagonal tension crack occurred suddenly in wider area. In addition, as the shear distance interval is shorter and the tension steel ratio is greater, the depth of the crack propagation at the flexural shear area was deeper than simple flexural area. Nonetheless, further propagation of diagonal crack did not occur due to the stirrup reinforcement. Although most specimen members showed a pattern of flexural compression failure, those test specimens (4B3-0.05, 4B3-0.1, and 7B3-0.05), which were designed with minimum steel content ratio, had their several (3~6) main cracks occur at a uniform interval. How-

Table 5 Test results of specimens.

No.	Beam ID	P_{cr} (kN)	Yield state				Maximum state			Ultimate state				ε_{cu}	$\frac{\delta_{u2}}{\delta_y}$	Failure mode
			P_{sy} (kN)	P_y (kN)	ε_{cr} (%)	δ_y (mm)	P_{max} (kN)	ε_{cmax} (%)	δ_{max} (mm)	P_{u1} (kN)	δ_{u1} (mm)	P_{u2} (kN)	δ_{u2} (mm)			
1	4B2-0.5	24.4	185.6	185.6	0.187	6.26	197.1	0.476	10.46	177.4	15.19	157.7	26.02	0.0051	4.16	FC
2	6B2-0.5	35.0	183.8	191.0	0.211	6.34	210.5	0.468	14.01	189.5	16.79	168.4	31.57	0.0047	4.97	FC
3	7B2-0.5	41.6	248.8	264.6	0.176	6.99	279.0	0.267	12.20	251.1	18.80	223.2	35.68	0.0028	5.10	FC
4	4B3-0.05	40.1	44.7	44.7	0.072	1.45	61.8	0.578	67.67	-	-	-	-	0.0059	46.67	FT
5	4B3-0.1	48.1	60.1	62.0	0.054	2.04	91.3	0.363	49.87	-	-	-	-	0.0037	24.45	FT
6	4B3-0.5	19.7	131.4	144.9	0.202	7.81	152.4	0.362	11.13	137.2	20.25	121.9	36.95	0.0057	4.73	FC
7	6B3-0.5	35.1	154.8	154.8	0.152	7.61	166.5	0.242	14.53	149.9	19.12	133.2	35.72	0.0024	4.97	FC
8	7B3-0.05	53.0	77.4	65.9	0.030	2.20	98.8	0.292	68.33	-	-	-	-	0.0031	31.06	FT
9	7B3-0.1	53.9	110.1	102.3	0.072	3.77	140.9	0.440	53.49	-	-	-	-	0.0046	14.19	FT
10	7B3-0.5	25.8	170.1	193.5	0.261	9.18	211.3	0.401	16.49	190.2	25.85	169.1	32.18	0.0040	3.51	FC
11	4B4-0.3	12.7	69.4	69.5	0.144	7.12	77.7	0.394	18.15	70.0	39.16	62.2	65.58	0.0043	9.21	FC
12	4B4-0.5	25.1	115.4	111.4	0.206	8.35	117.6	0.422	13.70	106.0	27.44	94.1	39.93	0.0047	4.78	FC
13	4B4-0.7	20.4	131.9	143.3	0.235	10.25	152.6	0.356	13.54	137.3	18.41	122.1	24.69	0.0050	2.41	FC
14	4B4-0.7(C0.2)	19.6	132.4	148.0	0.260	10.72	156.5	0.421	14.29	140.9	19.74	125.2	34.56	0.0045	3.22	FC
15	4B4-0.7(C0.3)	20.0	150.6	150.6	0.213	10.71	159.9	0.287	12.59	143.9	26.06	127.9	41.04	0.0039	3.83	FC
16	4B4-1.0	19.8	157.0	169.0	0.331	10.78	188.4	0.465	13.17	169.6	16.70	150.7	20.22	0.0048	1.88	FC
17	6B4-0.5	23.8	120.1	125.4	0.129	8.54	135.2	0.245	15.63	121.7	27.62	108.2	46.86	0.0034	5.49	FC
18	7B4-0.3	23.9	109.7	119.9	0.134	7.85	134.9	0.339	26.45	121.4	35.22	107.9	59.22	0.0034	7.54	FC
19	7B4-0.5	23.8	150.8	155.9	0.186	10.49	166.9	0.357	16.06	150.2	29.49	133.5	35.73	0.0039	3.41	FC
20	7B4-0.7	30.0	204.5	193.3	0.281	11.26	204.8	0.443	14.49	184.3	18.68	163.8	28.58	0.0070	2.54	FC
21	7B4-0.7(C0.2)	26.9	179.9	190.0	0.165	10.96	205.8	0.263	12.21	185.2	16.21	164.6	35.13	0.0037	3.21	FC
22	7B4-0.7(C0.3)	21.9	178.6	190.4	0.222	11.21	206.5	0.289	14.44	185.9	17.95	165.2	35.50	0.0036	3.17	FC
23	7B4-1.0	25.9	248.8	241.0	0.243	10.80	253.2	0.451	12.41	227.9	17.12	202.6	21.82	0.0045	2.32	FC

FC: Flexure-Compression, FT: Flexure-Tension

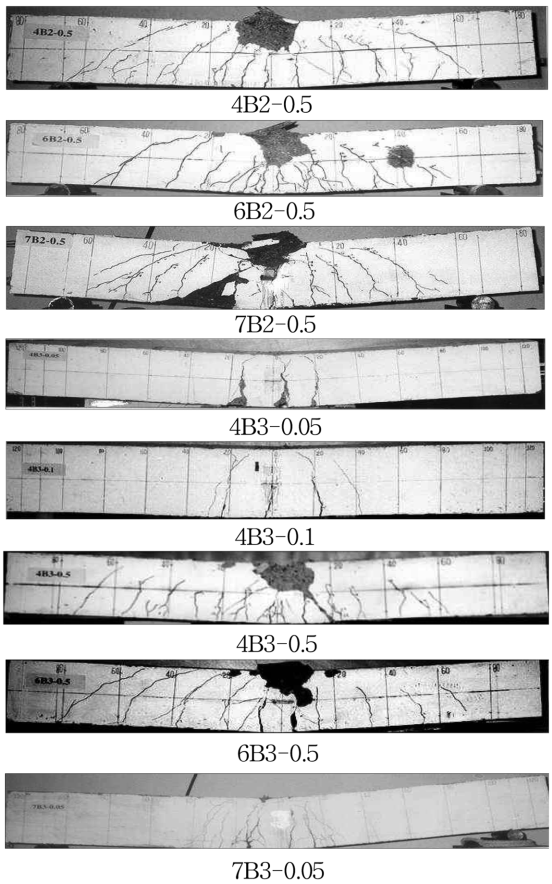

Fig. 3 Crack propagation and failure pattern.

ever, the cracks did not lead to the failure until the cracking reached the very end of the compression zone. Instead, those specimens showed a pattern of flexural tension failure, manifested by excessive cracking at the tensile side and subsequent failure.

3. Analysis of the experimental result and investigation of the ductility of high-strength concrete beams

3.1 Prediction equation for flexural strength of a concrete member by the ACI-318 code and verification of the stress distribution model

Table 6 shows the comparison among the experimental results of this study and the prediction results from the prediction equation for the flexural strength by ACI-318 code and the prediction by stress distribution model as proposed by Ibrahim, et. al[2]. and Jang, I. Y., et. al.[3]

Fig. 6 shows the accuracy of ACI bending strength computational equation by various tensile reinforcement ratios (ρ_t / ρ_b).

As shown in the comparison result, there was no noticeable change or difference by the stress block pattern for all steel beams across under- and excessive tension steel ratios. Fig. 4 shows that the safety of high-strength concrete beam was reduced with the increases in concrete compressive strength and tension steel ratio according to the equivalent rectangular model of ACI-318. However, at the range of $\rho_t / \rho_b \leq 1.0$, the bending strength of high-strength concrete beam is predicted in the safe side overall. Thus, it is deemed that the ACI-318 computational equation for flexural

Table 6 Test result of specimens.

Beam ID	f_c (MPa)	$M_{n,test}$ (kN·m)	$M_{n,test}$ / $M_{n,cal}$		
			ACI-318	Ibrahim	Jang
4B2-0.5	40	51.74	1.139	1.151	1.150
6B2-0.5	60	55.26	1.162	1.173	1.176
7B2-0.5	70	73.24	1.158	1.172	1.177
4B3-0.05	40	29.66	1.628	1.632	1.632
4B3-0.1	40	43.68	1.362	1.367	1.367
4B3-0.5	40	51.21	1.127	1.139	1.139
6B3-0.5	60	55.94	1.176	1.188	1.190
7B3-0.05	70	46.85	1.447	1.453	1.454
7B3-0.1	70	67.63	1.402	1.408	1.409
7B3-0.5	70	71.00	1.123	1.136	1.141
4B4-0.3	40	32.63	0.993	1.001	1.001
4B4-0.5	40	49.39	1.087	1.098	1.098
4B4-0.7	40	64.09	1.100	1.114	1.113
4B4-0.7(C0.2)	40	65.73	1.128	1.142	1.142
4B4-0.7(C0.3)	40	67.16	1.153	1.167	1.167
4B4-1.0	40	79.13	1.120	1.147	1.146
6B4-0.5	60	56.78	1.194	1.205	1.208
7B4-0.3	70	56.66	1.176	1.189	1.192
7B4-0.5	70	70.10	1.108	1.122	1.127
7B4-0.7	70	86.02	1.054	1.078	1.086
7B4-0.7(C0.2)	70	86.44	1.059	1.083	1.091
7B4-0.7(C0.3)	70	86.73	1.062	1.087	1.095
7B4-1.0	70	106.34	1.030	1.063	1.074
		Ave.	1.164	1.168	1.170
		St. Dev.	0.140	0.137	0.136

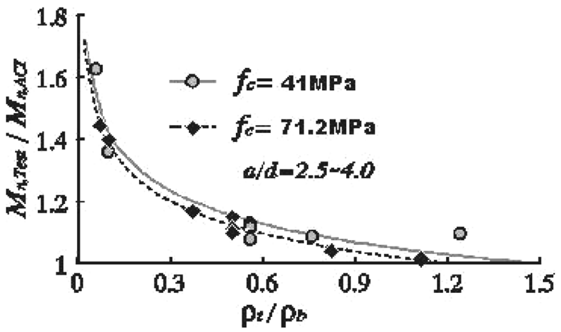

Fig. 4 Accuracy of ACI bending strength calculation for various tensile reinforcement ratios (ρ_t/ ρ_b).

(bending) strength can still be applied to high-strength concrete beam in design and analysis of ultimate strength along with the applied strength reduction coefficient. Additionally, the computed values from the quadrangle model of Ibrahim et. al.[2] and trapezoid model of Jang I. Y., et. al.[3] are evaluated to be on the safer side than the predicted values from ACI-318 equation. Moreover, the deviation of the predicted values was relatively stable.

3.2 Flexural ductility

3.2.1. Examination of ductility index computation methods

It is not easy to clearly define the yield point from load-displacement relationship due to the following points. The time to reach the yield state by the loading stage varies with the nonlinear behavior of the materials and the location of each steel reinforcement at the cross section of the member, and the location of plastic hinge occurrence due to the load increase differs from the overall perspective of the member. This study selected the computational method shown in Fig. 5(a), which is one of many existing methods of defining yield displacement. The computational method illustrated in Fig. 5(a) is an effective way of expressing the reduced stiffness of entire member due to cracking when the member reaches the boundary of elasticity. It is deemed to be the most realistic method of computing the yield displacement of steel concrete structures.

Additionally, the computational method illustrated in Fig .5(b) is deemed the most realistic and rational way of defining the ultimate displacement, i.e. the point of failure of steel concrete member as used in many studies. It defines the ultimate displacement at the point of 80% of the maximum load after reaching the load peak.

3.2.2. Comparison of the flexural ductility behavior by the experimental variables

(1) Influence of concrete compressive strength and tensile reinforcement ratio

The ductile behaviors of high-strength concrete beam members with various concrete compressive strengths (40, 60, 70 MPa) and tensile reinforcement ratios are compared in Fig. 8~10 based on the results of this research. As seen in Fig. 6, when the tensile reinforcement ratio is the same, the load-deflection behavior prior to the yield of tensile reinforcement hardly change with the change in compressive strength, but it varies greatly after the yield. The increase in deflection varies proportionally with the load increase. Thus, the general trend of increasing ductility with the increase in concrete strength is observed. The bending strength increased by about 20% as the compressive strength increased from 40 MPa to 60 MPa regardless of *a*/*d* ratio. However, it remained almost the same when the test specimen of 60 MPa was compared with the specimen of 70 MPa. Thus, it was verified that high-strength concretes was effective in improving the ductility of the member, given the same tensile reinforcement ratio, as shown in Fig. 7, without the negative effect of lowered bearing capacity against bending force due to lowered ρ_t/ ρ_b. Fig. 8 shows typical ductility reduction of a flexural member owing to the increase in ρ_t/ρ_b. The increase in concrete compressive strength under the same condition also results in the increase in stiffness and bending (flexural) strength due to the increase in tensile reinforcement. However, the rapid decrease in bearing capacity after the maximum strength makes the increase in the ductility of the member difficult or can cause even the tendency for reduced ductility.

(2) Influence of shear span to beam depth ratio

The moment-curvature behavior of the cross section can not

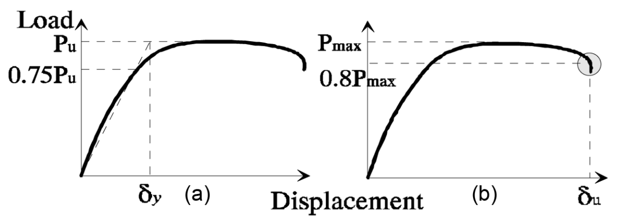

Fig. 5 Method of defining yield displacement and ultimate state (a) based on reduced stiffness equivalent elastic-plastic yield (b) based on 0.8 P_{max}.

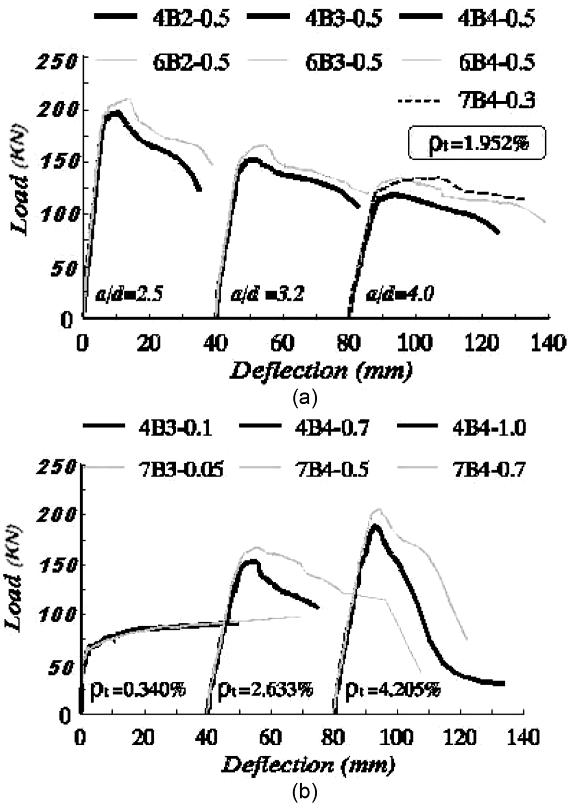

Fig. 6 Comparison of ductile behavior of high-strength concrete beam members with various tensile reinforcement ratios.

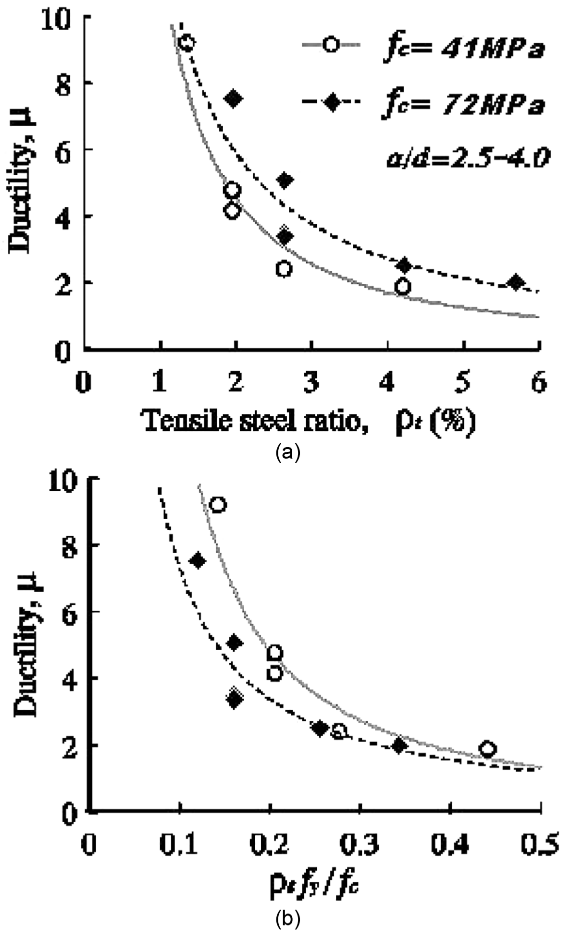

Fig. 7 Relationship between ductility and tensile steel ratio.

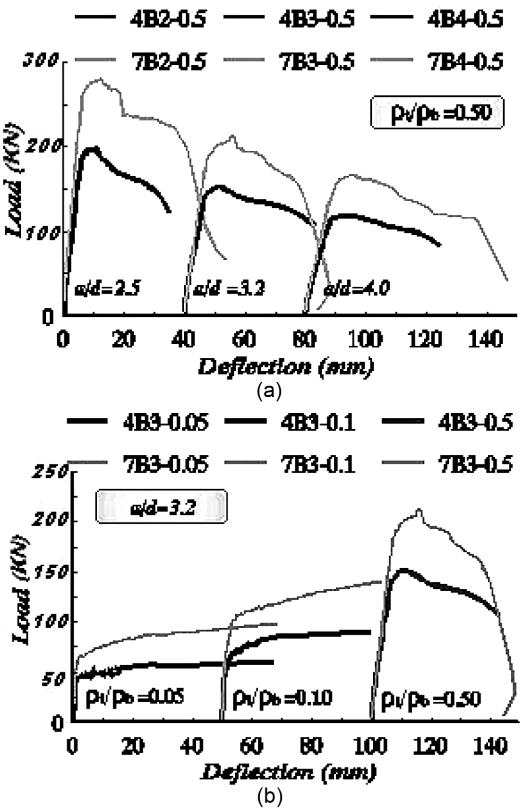

Fig. 8 Comparison of balanced steel ratio and compression strength with respect to load-deflection behavior of beam member.

evaluate the ductility. Generally, the increase in *a*/*d* changes the behavior of the member from shear to flexure and increases the ductility of the member.

As seen from the experimental result of $\rho_t / \rho_b = 0.5$ in Fig. 9, the strength and initial stiffness increase greatly as *a*/*d* decreases. However, the flexural failure of the concrete member with shorter *a*/*d* on the compressive side occurs rapidly, showing that the concrete beam member becomes more brittle after the maximum loading for the member with shorter *a*/*d*. Additionally, the bearing capacity to flexural force decreases rapidly after the maximum loading as the concrete compressive strength increases, given the same *a*/*d* condition.

The experimental result on the deflection ductility of the mem-

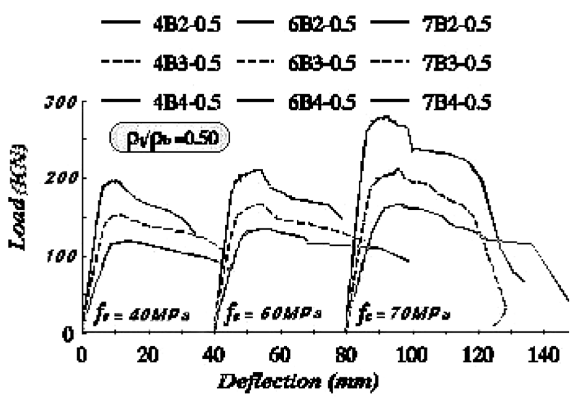

Fig. 9 Comparison of the load-deflection relationship for beam members of various shear span ratios, compressive strengths and tensile reinforcement ratio of $\rho_t / \rho_b = 0.5$

ber showed that there was no rapid increase in ductility along with the increase in *a*/*d*. On the contrary, the ductility decreased along with the increase in *a*/*d* for the member of $f_c = 71$ MPa. It is thus construed that the influence of *a*/*d* on the ductility of the member is not so great as the concrete compressive strength and the reinforcement ratio. Nevertheless, it is affirmed as shown in Fig. 10 that the ductility increases with the increase in *a*/*d*, given the condition of the same concrete compressive strength and tensile reinforcement ratio.

(3) Influence of web reinforcement ratio

Pastor et. al.[4)] reported in their experimental investigation of doubly reinforced beam of about 60 MPa compressive strength that the deflection ductility can be greatly enhanced by the installation of compression bars or reinforcing bars in the flexural zone compared to the use of single reinforcement. Moreover, they reported that the compression bar was more effective in enhancing the deflection ductility compared to flexural rebars.

Figure 11 shows the change in flexural strength and ductility by the use of compression bars. In general, the increase in stiffness or flexural strength owing to the use of compression bars was not so noticeable, and a rapid reduction in load capacity due to the ductility increase (caused by the increased use of compression bars) and failure of the concrete in the compressive side after the maximum load was clearly observed in the experimental specimen of 40 MPa compressive strength (4B4-0.7). Although the ductility of the test specimen of 70 MPa compression strength (7B4-0.7) increased, a rapid reduction in load capacity was observed despite of the compression bars due to the increased brittle failure in the compressive side (caused by the increase in compressive strength of the concrete).

Since it was not sufficient to investigate the flexural (bending) strength (measured by deflection) and ductility of the doubly reinforced beam with the data of this experiment alone, previous experimental data of Pastor et. al.[4] and Jang, et. al.[3] as summarized in Table 7 were analyzed, and the analysis result is depicted in figure 11.

Figure 12 shows the ductility and flexural strength increase with compression bar index ($\rho_c f_{cy}/f_c$) for doubly reinforced beams and beams of single reinforcement (compression bar ratio of $\rho_c = 0$). Figure 12(a) shows the ductility is greatly enhanced as the compression bar index increases compared to the beam of single rein-

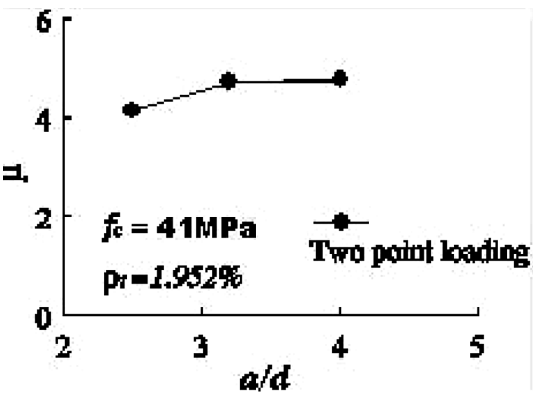

Fig. 10 Effect of ductility on shearing.

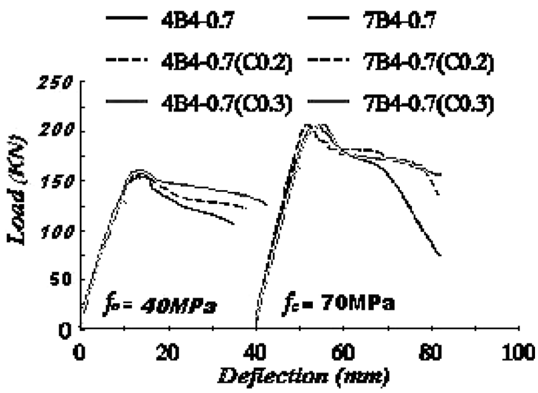

Fig. 11 Comparison of load-deflection relationship for beam members of 0.7 ρ_b and various compression bar ratios.

Table 7 Basic experiment result for beams of double reinforcement.

Ref.	ID	Section b × d (mm)	a/d	f_c (MPa)	Tension bar			Hoops			Comp. bar		M_{max} (kN·m)	μ
					f_y (MPa)	ρ_s (%)	ρ_s/ρ_b	f_{wy} (MPa)	s (mm)	ρ_w (%)	f_{cy} (MPa)	ρ_c (%)		
Present study	4B4-0.7	140×210	4.0	41	435	2.63	0.76	395	100	1.02	435	0	64.1	2.41
	4B4-0.7(C0.2)	140×210	4.0	41	435	2.63	0.76	395	100	1.02	435	0.49	6..7	3.22
	4B4-0.7(C0.3)	140×210	4.0	41	435	2.63	0.76	395	100	1.02	435	0.86	67.2	3.83
	7B4-0.7	140×210	4.0	71	450	4.21	0.80	395	100	1.02	450	0	86.0	2.54
	7B4-0.7(C0.2)	140×210	4.0	71	450	4.21	0.80	395	100	1.02	450	0.78	86.4	3.21
	7B4-0.7(C0.3)	140×210	4.0	71	450	4.21	0.80	395	100	1.02	450	1.42	86.7	3.17
Pastor et al. (1984)	A-1	186×272	4.49	26	485	1.1	0.52	395	127	0.27	0	0	69	3.68
	A-2	184×270	4.52	46	485	1.7	0.53	395	127	0.27	0	0	103	2.66
	B-1	176×272	4.49	60	436	2.4	0.43	395	63.5	0.57	485	1.2	133	2.35
	B-3	175×275	4.44	60	436	2.4	0.46	395	63.5	0.57	485	1.2	138	4.54
	B-4	170×273	4.47	60	436	2.5	0.36	395	63.5	0.59	436	2.5	165	8.45
	B-5	178×270	4.52	60	436	2.4	0.43	395	63.5	0.56	485	1.2	139	5.52
	B-6	175×270	4.52	60	436	2.5	0.36	395	63.5	0.57	436	2.5	152	6.26
Jang et al. (1992)	No.1	200×350	3.6	105	570	1.23	0.09	0	0	0	0	0	75	11.0
	No.3	200×350	3.6	103	533	1.66	0.13	0	0	0	402	0.09	69	11.1
	No.4	200×350	3.6	103	570	1.23	0.09	0	0	0	402	0.09	103	12.4
	No.7	200×350	3.6	98	570	1.23	0.09	387	90	0.79	402	0.09	165	14.3

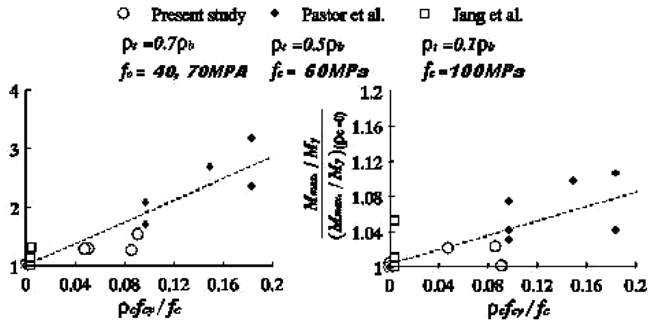

(a) Ductility enhancement (b) Beam moment enhancement

Fig. 12 Comparison of bending strength and ductile quality of beam members of high strength concrete by compressive reinforcement index $(\rho_c f_{cy} / f_c)$

the yield of the member increases by 2~8% compared to the beam of single reinforcement as the compression bar index increases. Thus, the compression bars has the role of enhancing the ductility of a concrete member after the yield of the member by improving the redistribution of the plastic moment in the plasticity range to a certain extent based on the experimental findings. This observation signifies that the increase in flexural strength to induce a flexural plastic hinge in the beam member should be based on the increase in the quantity of compression bars in anti-seismic design of the joint between concrete beam and column.

4. Conclusions

The following conclusions are derived from this experimental study.

1) Although the equivalent rectangular model of ACI-318 code resulted in reduced safety due to the increases in concrete compressive strength and tensile reinforcement ratio, it was verified that it generally predicted the flexural (bending) strength of a high-strength concrete beam in the relatively safe (conservative) side at the range of $\rho_t / \rho_b \leq 1.0$.

2) It is more realistic and reasonable to define the yield displacement of the high-strength concrete member for the computation of its ductility index at the point of yield displacement from equivalent elasticity-plasticity relationship of secant elastic stiffness to 75% of the maximum load and as the ultimate displacement at the point of 80% of the maximum load after the maximum (peak) load.

3) The degree of influence of the variables on the ductility of high-strength concrete beam member was ranked to be tensile reinforcement ratio, compression bar ratio, transverse reinforcement ratio at the transverse compressive side, shear span ratio, and concrete compressive strength in descending order. Additionally, the flexural (bending) strength of high-strength concrete beam member could be predicted by the tensile reinforcement ratio, compression bar ratio, and concrete compressive strength in the descending order of importance.

Acknowledgements

This paper was supported by Research Fund, Kumoh National Institute of Technology. The authors hereby express their sincere appreciation for the support.

References

1. Leslie, K. E., Rajagopalan, K. S., and Eveard, N. J., “Flexural Behavior of High-Strength Concrete Beams,” *ACI Journal*, Vol. 73, No. 8, 1976, pp. 517~521.

2. Ibrahim, H. H. H. and MacGregor, J. G., “Modification of the ACI Rectangular Stress Block for High-Strength Concrete,” *ACI Structural Journal*, Vol. 94, No. 1, 1997, pp. 40~48.

3. Jang, I. Y. and Park, H. G., “Development of Stress-Strain Model and Stress Distribution Model for Ultra-Strength Concrete,” *Journal of Korea Concrete Institute*, Vol. 9, No. 5, October 1997.

4. Pastor, J. A., Nilson, A. H., and Slate, F. O., “Behavior of High-Strength Concrete Beams,” Research Report 84-3, Department of Structural Engineering, Cornell University, Ithaca, New York, February, 1984, 311 pp.